ChemPubSoc Europe

DOI: 10.1002/chem.201600622

CHEMISTRY
A European Journal
Full Paper

Cluster Compounds |*Hot Paper*|

Diverse Ligand-Functionalized Mixed-Valent Hexamanganese Sandwiched Silicotungstates with Single-Molecule Magnet Behavior

Han Xue,[a] Jun-Wei Zhao,*[b] Rui Pan,[a] Bai-Feng Yang,[a] Guo-Yu Yang,*[a, c] and
Hong-Sheng Liu*[d]

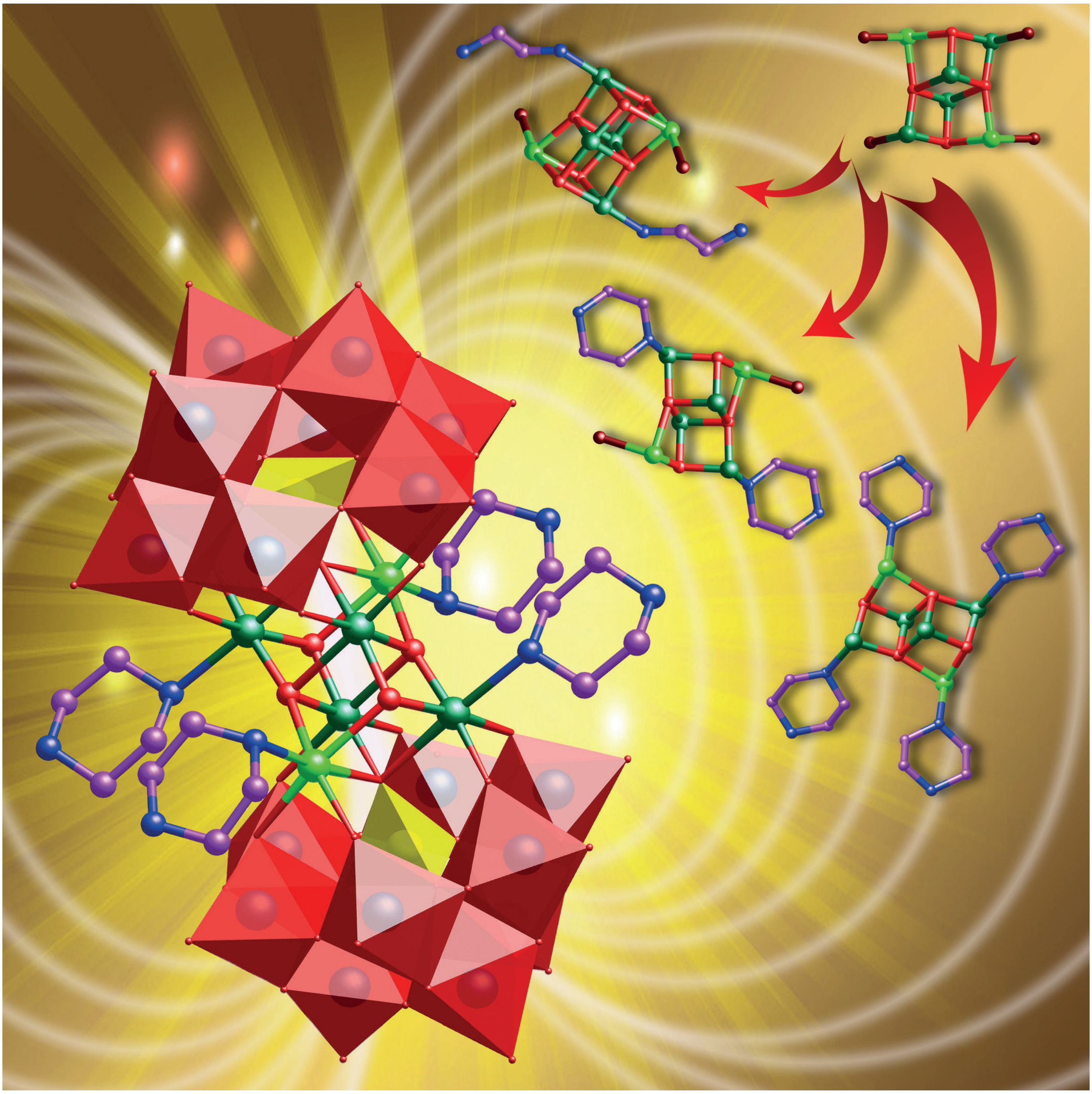

© 2016 Wiley-VCH Verlag GmbH & Co. KGaA, Weinheim

Abstract: Under hydrothermal conditions, replacement of the water molecules in the $[Mn^{III}_4Mn^{II}_2O_4(H_2O)_4]^{8+}$ cluster of mixed-valent Mn_6 sandwiched silicotungstate $[(B\text{-}\alpha\text{-}SiW_9O_{34})_2Mn^{III}_4Mn^{II}_2O_4(H_2O)_4]^{12-}$ (**1 a**) with organic N ligands led to the isolation of five organic–inorganic hybrid, Mn_6-substituted polyoxometalates (POMs) **2**–**6**. They were all structurally characterized by IR spectroscopy, elemental analysis, thermogravimetric analysis, diffuse-reflectance spectroscopy, and powder and single-crystal X-ray diffraction. Compounds **2**–**6** represent the first series of mixed-valent $\{Mn^{III}_4Mn^{II}_2O_4(H_2O)_{4-n}(L)_n\}$ sandwiched POMs covalently functionalized by organic ligands. The preparation of **1**–**6** not only indicates that the double-cubane $\{Mn^{III}_4Mn^{II}_2O_4(H_2O)_{4-n}(L)_n\}$ clusters are very stable fragments in both conventional aqueous solution and hydrothermal systems and that organic functionalization of the $[Mn^{III}_4Mn^{II}_2O_4(H_2O)_4]^{8+}$ cluster by substitution reactions is feasible, but also demonstrates that hydrothermal environments can promote and facilitate the occurrence of this substitution reaction. This work confirms that hydrothermal synthesis is effective for making novel mixed-valent POMs substituted with transition-metal (TM) clusters by combining lacunary Keggin precursors with TM cations and tunable organic ligands. Furthermore, magnetic measurements reveal that **3** and **6** exhibit single-molecule magnet behavior.

Introduction

Polyoxometalates (POMs) are a class of discrete anionic clusters with oxo bridges between early transition metal (TM) atoms in high oxidation states (usually Mo^{VI}, W^{VI}, V^{V}, Nb^{V}, or Ta^{V}).[1a–c] In this field, TM-substituted POMs (TMSPs) have attracted extensive interest due to their flexible and diverse structures, enormous compositional and electronic tunability, and widespread potential applications in catalysis, electronics, magnetism, and analytical chemistry.[1–3] Their particular structural characteristics suggest that TMSP-based materials are good candidates for the designed construction of electronically and magnetically interesting materials. Since the discovery of a great variety of lacunary Keggin-type $[XW_{12}O_{40}]^{n-}$ ($X = P^{V}/As^{V}/Si^{IV}/Ge^{IV}$) and Dawson-type $[\alpha\text{-}X_2W_{18}O_{62}]^{6-}$ ($X = P^{V}/As^{V}$) polyoxoanions (POAs), the discovery and investigation of their TM-substituted lacunary derivatives have been an significant focus in POM chemistry,[4a–c] because these lacunary POM precursors have high reactivity and can act as good donors to coordinate to electrophilic TM cations.[4d] Moreover, the high capacity of lacunary POAs to encapsulate magnetic TM clusters between nonmagnetic POM matrices makes them especially valuable for analyzing magnetic interactions.[4e,f]

The interest in Mn complexes is particularly high due to their remarkable magnetic properties, such as single-molecule magnet (SMM) behavior. During the past two decades, some SMMs have been made by supporting organic ligands such as carboxylates, alkoxides, and amines.[5] A pioneering work in this area was the discovery of $[Mn_{12}(CH_3COO)_{16}(H_2O)_4O_{12}]$ (Mn_{12}) in 1980, the SMM behavior of which was proved by Gatteschi et al. after 13 years.[5d,6] Lacunary POMs can be considered to be inorganic multidentate ligands for incorporating Mn ions into their skeletons and constructing novel magnetic manganese-substituted polyoxometalates (MSPs).[7] In the past few years, some POM-based SMMs have been obtained,[8–10] and some mixed-valent MSP-based SMMs are $\{[GeW_9O_{34}]_2[Mn^{III}_4Mn^{II}_2O_4(H_2O)_4]\}^{12-}$,[9a] $\{[SiW_9O_{34}]_2[Mn^{III}_4\text{-}Mn^{II}_2O_4\text{-}(H_2O)_4]\}^{12-}$,[9a] $[(\alpha\text{-}P_2W_{15}O_{56})Mn^{III}_3Mn^{IV}O_3(CH_3COO)_3]^{8-}$,[9b] $[(\alpha\text{-}P_2W_{15}O_{56})_2Mn^{III}_6Mn^{IV}O_6(H_2O)_6]^{14-}$,[9c] $[(A\text{-}\beta\text{-}SiW_9O_{34})Mn^{III}_3Mn^{IV}O_3\text{-}(CH_3COO)_3]^{6-}$,[9d] and $\{[Mn^{IV}_2Mn^{III}_6Mn^{II}_4(\mu_3\text{-}O)_6(\mu\text{-}OH)_4(H_2O)_2(CO_3)_6][B\text{-}\beta\text{-}SiW_6O_{26}]_2\}^{18-}$.[2c] Most of the reported MSP-based SMMs contain mixed-valent MnO cubane units, which play an important role in the design and preparation of new MSP aggregates with SMM behavior. The above-mentioned SMMs were made in conventional aqueous solution. On the contrary, the design and synthesis of new MSP-based SMMs under hydrothermal conditions remain largely unexplored, although the hydrothermal technique has been proven to be a particularly powerful synthetic approach. By combining the synthetic strategy of lacunary POM precursors with the hydrothermal technique, we have obtained a series of intriguing high-nuclearity TMSPs.[4b,d,11] Inspired by these results, we decided to utilize this strategy to make new Keggin-type MSP-based SMMs. First, a mixed-valent $[Mn^{III}_4Mn^{II}_2O_4(H_2O)_4]^{8+}$ cluster sandwiched in silicotungstate $(H_3deta)_4[(B\text{-}\alpha\text{-}SiW_9O_{34})_2Mn^{III}_4Mn^{II}_2O_4(H_2O)_4]\cdot 8\,H_2O$ (**1**, deta = diethylenetriamine) was made, which consists of a $[Mn^{III}_4Mn^{II}_2O_4(H_2O)_4]^{8+}$ cluster anchored to two trilacunary Keggin $[B\text{-}\alpha\text{-}SiW_9O_{34}]^{10-}$ fragments. There are four coordinated water molecules in the mixed-valent $[Mn^{III}_4Mn^{II}_2O_4(H_2O)_4]^{8+}$

---

[a] H. Xue, R. Pan, Prof. B.-F. Yang, Prof. Dr. G.-Y. Yang
MOE Key Laboratory of Cluster Science
School of Chemistry
Beijing Institute of Technology
Beijing 100081 (P. R. China)
E-mail: ygy@bit.edu.cn

[b] Prof. Dr. J.-W. Zhao
Henan Key Laboratory of Polyoxometalate Chemistry
College of Chemistry and Chemical Engineering
Henan University
Kaifeng, Henan 475004 (P. R. China)
E-mail: zhaojunwei@henu.edu.cn

[c] Prof. Dr. G.-Y. Yang
Department of Chemistry
Key Laboratory for Preparation and Application
of Ordered Structural Materials of Guangdong Province
Shantou University
Shantou, Guangdong 515063 (P. R. China)

[d] Prof. Dr. H.-S. Liu
Key Laboratory of Oilfield Applied Chemistry
College of Heilongjiang Province
Daqing Normal University
Daqing, Heilongjiang 163712 (P. R. China)
E-mail: hsliu@126.com

Supporting information for this article is available on the WWW under http://dx.doi.org/10.1002/chem.201600622.

© 2016 Wiley-VCH Verlag GmbH & Co. KGaA, Weinheim

cluster in **1**. According to our research concept that coordinated water molecules in the Ni_6-substituted POM $[Ni_6(\mu_3\text{-}OH)_3(H_2O)_6L_3(B\text{-}\alpha\text{-}PW_9O_{34})]$ [L = ethylenediamine (en), dap = 1,2-diaminopropane (dap)] can be substituted by N or O atoms of organic ligands,[11a,d,g] we assumed that the aqua ligands of the $[Mn^{III}_4Mn^{II}_2O_4(H_2O)_4]^{8+}$ cluster in **1** could also provide the possibility of forming organic–inorganic hybrid $\{Mn^{III}_4Mn^{II}_2O_4(H_2O)_{4-n}(L)_n\}$ (L = organic ligands) clusters by replacing water molecules with organic ligands. Thus, we tried to find suitable ligands to replace these water molecules in the $[Mn^{III}_4Mn^{II}_2O_4(H_2O)_4]^{8+}$ ($Mn^{III}_4Mn^{II}_2$) cluster core of **1** to prepare organic–inorganic hybrid mixed-valent, hexa-Mn $\{Mn^{III}_4Mn^{II}_2O_4(H_2O)_{4-n}(L)_n\}$ cluster-sandwiched silicotungstates and investigate the influence of the substitution of organic ligands on their magnetic behavior. Five organic–inorganic hybrid $\{Mn^{III}_4Mn^{II}_2\}$ cluster-sandwiched silicotungstates $[H_2en]_5[(B\text{-}\alpha\text{-}SiW_9O_{34})_2Mn^{III}_4Mn^{II}_2O_4(H_2O)_2(Hen)_2]\cdot 8\,H_2O$ (**2**), $[H_2ppz]_4\text{-}[H_21,3\text{-}dap]_2[(B\text{-}\alpha\text{-}SiW_9O_{34})_2Mn^{III}_4Mn^{II}_2O_4(H_2O)_2(ppz)_2]\cdot 6\,H_2O$ (**3**), $H_2[H_2ppz]_4[(B\text{-}\alpha\text{-}SiW_9O_{34})_2Mn^{III}_4Mn^{II}_2O_4(H_2O)_2(Hppz)_2]\cdot 8\,H_2O$ (**4**), $[H_2ppz]_3[H_3deta]_2\ [(B\text{-}\alpha\text{-}SiW_9O_{34})_2Mn^{III}_4Mn^{II}_2O_4(ppz)_4]\cdot 12\,H_2O$ (**5**), and $[H_2ppz]_2[H_2en]_2\ [(B\text{-}\alpha\text{-}SiW_9O_{34})_2Mn^{III}_4Mn^{II}_2O_4(Hppz)_4]\cdot en\cdot 10\,H_2O$ (**6**) (ppz = piperazine, 1,3-dap = 1,3-diaminopropane) were prepared under hydrothermal conditions. As expected, the hybrid skeletons of **2**–**6** feature two trivacant $[B\text{-}\alpha\text{-}SiW_9O_{34}]^{10-}$ fragments sandwiching an interesting organic–inorganic hybrid, mixed-valent, hexa-Mn $\{Mn^{III}_4Mn^{II}_2O_4\ (H_2O)_{4-n}(L)_n\}$ cluster, and are the first examples of mixed-valent $\{Mn^{III}_4Mn^{II}_2\}$-substituted sandwich-type POMs functionalized by organic ligands. The successful obtainment of **2**–**6** also offers us the possibility of introducing bridging organic ligands to replace water molecules and construct mixed-valent, Mn-cluster-encapsulating, organic–inorganic hybrid magnetic frameworks. Moreover, the optical and thermogravimetric properties of **1**–**6** and magnetic properties of **3** and **6** were investigated.

Results and Discussion

Synthesis and spectroscopic characterization

In the past several decades, many MSPs have been obtained by the conventional aqueous-solution reaction of lacunary POM precursors with Mn^{2+} ions at atmosphere pressure and room temperature. Although the conventional solution strategies for making TMSPs have been well developed, the use of the hydrothermal technique to prepare MSP-based SMMs is still in its infancy. In the past few years, the hydrothermal technique has proved to be an extraordinarily powerful synthetic method for creating novel organic–inorganic hybrid materials in the POM field. Because of the high pressure and temperature exerted by hydrothermal environments, the reaction system can shift from the thermodynamic to the kinetic regime to capture more complicated metastable phases, and the solubility of different phases is increased, so that various organic components can be easily introduced, and novel products that cannot be obtained in conventional aqueous solution may result.[12] Therefore, we have developed synthetic strategies combining the hydrothermal technique with lacunary POM precursors in the presence of various TM ions and different organic ligands to construct high-nuclearity TMSPs since 2007, and a large number of intriguing organic–inorganic hybrid, high-nuclearity TMSPs have been discovered.[4b,d,11] Besides these high-nuclearity Cu-/Ni-substituted POM hybrids, we introduced Mn^{2+} ions into our system and launched a systematic exploration of the reaction of trivacant POM precursors with Mn^{2+} ions in the presence of organic amine ligands under hydrothermal conditions, because Mn^{2+} ions are prone to be oxidized to high- or mixed-valent Mn ions and can then be encapsulated into POM matrixes with formation of multi-Mn-substituted POMs having interesting physicochemical properties. Moreover, they have relatively high spins and negative single-axis magnetic anisotropy, which help to construct multifunctional magnetic materials.

In a specific hydrothermal system, multiple factors such as the concentration and type of reactants, pH, temperature, reaction time, and additives can affect the reaction, crystallization, and the resulting products. We obtained a series of novel organic–inorganic hybrid, mixed-valent, $\{Mn^{III}_4Mn^{II}_2\}$-sandwiched POMs by hydrothermal synthesis with tunable control of Mn^{2+} ions, organic amine ligands, pH, and temperature. Initially, unexpected sandwich-type dimeric silicotungstate **1** containing an $\{Mn^{III}_4Mn^{II}_2\}$ core in the central belt was prepared by treating $[A\text{-}\alpha\text{-}SiW_9O_{34}]^{10-}$ with $Mn(NO_3)_2\cdot 4\,H_2O$ at 60 °C in the presence of deta and 4,4′-bipyridine (4,4′-bpy). An excess of $Mn(NO_3)_2\cdot 4\,H_2O$ was used to enhance its ability to react with $[A\text{-}\alpha\text{-}SiW_9O_{34}]^{10-}$ and shift the reaction in the direction of the desired products. Under similar conditions, en/ppz was utilized to replace deta in the anticipation of obtaining similar species to **1**; however, this failed. By increasing the temperature to 80 °C and simultaneously introducing *N*-(3-aminopropyl)morpholine (apm) into the system, the reaction of $[A\text{-}\alpha\text{-}SiW_9O_{34}]^{10-}$ with $Mn(NO_3)_2\cdot 4\,H_2O$ in the presence of en and apm led to the isolation of **2**. Interestingly, the skeleton of **2** is analogous to the $[(B\text{-}\alpha\text{-}SiW_9O_{34})_2Mn^{III}_4Mn^{II}_2O_4(H_2O)_4]^{12-}$ unit in **1** except that two water ligands in **1** were replaced by two end-on en molecules. It is noteworthy that **2** can not be obtained under the same conditions without apm, which indicates that apm plays an important synergistic role in the formation of **2**, although it is not found in the final structure of **2**. For the preparation of **3**, 1,3-dap and ppz were employed as organic amine ligands instead of en and apm in **2**, $Mn(NO_3)_2\cdot 4\,H_2O$ was replaced by $MnSO_4\cdot 2\,H_2O$, and the reaction temperature was elevated to 90 °C. Compound **3** with a similar skeleton to **2** was obtained by the substitution of en by ppz. When deta replaced 1,3-dap and $Mn(NO_3)_2\cdot 4\,H_2O$ was still used as the starting material under similar conditions to the synthesis of **3**, compound **4** was isolated. Its structure closely resembles that of **3**, and the main distinction between them lies in the surrounding countercations. Moreover, to further explore the influence of other amines on the architectures in the system, deta was replaced by 1,6-hexanediamine or 4,4′-bpy under the same conditions; however, only amorphous precipitates were obtained. It can be speculated that the size of the organic molecules may have an important effect on the formation of the target products. In

© 2016 Wiley-VCH Verlag GmbH & Co. KGaA, Weinheim

the structures of **1**–**4**, two out of four water ligands in the $[Mn^{III}_4Mn^{II}_2O_4(H_2O)_4]^{8+}$ cluster core have been substituted by en or ppz ligands, so we wondered whether all four active sites could be replaced by organic ligands. Hence, we further increased the reaction temperature and the concentration of ppz. After systematic exploration, **5** was obtained, in which the four water ligands are completely replaced by ppz ligands. To further investigate the assembly mechanism and structural diversity that can be tuned by different organic ligands, we extended our studies from deta to en and isolated another tetrappz-substituted hexa-Mn-sandwiched silicotungstate, namely, **6**. Unfortunately, a similar structure to **2** in which the other two water ligands were also replaced by en ligands could not be isolated to date. It can be concluded that the type (size and shape) of organic amines contributes to the construction of diverse structures. Currently, studies on using $[A\text{-}\alpha\text{-}PW_9O_{34}]^{9-}$ or $[A\text{-}\alpha\text{-}GeW_9O_{34}]^{10-}$ instead of $[A\text{-}\alpha\text{-}SiW_9O_{34}]^{10-}$ are in progress.

From the viewpoint of synthetic conditions, besides the above-mentioned factors, other factors were also taken into consideration. On the one hand, the pH value of the reaction system significantly influences the final products. The initial pH values of **1**–**2** were restricted to a relatively narrow range of 7.5–8, whereas the starting pH values of **3**–**6** were in a relatively wide range of 8.5–10, from which we infer that the basicity of ligands contributes to the formation of **1**–**6** to a large extent. On the other hand, a series of systematic studies showed that **2**–**6** can not be prepared in conventional aqueous solution from the same starting materials. In conclusion, the vacant sites of the A-α-SiW_9 segment as structure-directing agent effectively induce the formation of Mn clusters and stabilize the final structure, while the organic ligands containing N-donor sites that function as structure-stabilizing agents are excellent candidates for reaction with electrophilic Mn cations to generate Mn complexes and concurrently enhance the stability of the product. In other words, the mechanism of the reaction is still not thoroughly understood up to now.

The IR spectra of **1**–**6**, recorded on KBr pellets in the range of 4000–400 cm^{-1} (Figure S1 in the Supporting Information), display the characteristic $\nu_{as}(Si{-}O_a)$, terminal $\nu_{as}(W{-}O_t)$, corner-sharing $\nu_{as}(W{-}O_b)$, and edge-sharing $\nu_{as}(W{-}O_c)$ vibrational bands of the trivacant Keggin-type silicotungstate framework.[13] Groups of vibrational bands at 942–940, 981–985, 887–874, 780–774, and 704–708 cm^{-1} are attributed to the $\nu(Si{-}O_a)$, $\nu(W{-}O_t)$, $\nu(W{-}O_a)$, $\nu(W{-}O_b)$, and $\nu(W{-}O_c)$ modes, respectively. Compared with the trivacant Keggin-type precursor $Na_{10}[\alpha\text{-}SiW_9O_{34}]\cdot 18\,H_2O$, the $\nu(W{-}O_{b,c})$ vibrational bands of **1**–**6** have different shifts, which are related to incorporation of the $\{Mn^{III}_4Mn^{II}_2\}$ cluster core into the vacancies of the $[\alpha\text{-}SiW_9O_{34}]^{10-}$ fragments. The bands appearing at 3246–3224 and 3120–3008 cm^{-1} are assigned to the $\nu(NH_2)$ and $\nu(CH_2)$ stretching vibrations, whereas the those at 1622–1507 and 1496–1310 cm^{-1} correspond to the $\delta(NH_2)$ and $\delta(CH_2)$ bending vibrations, respectively. The occurrence of these characteristic bands confirms the presence of organic groups in **1**–**6**. In addition, the vibrational bands centered at 3434–3414 cm^{-1} are indicative of the presence of lattice water molecules or coordinated water molecules.

To evaluate the optical properties of **1**–**6**, the diffuse-reflectance spectra for powdered crystal samples were measured to obtain their bandgaps E_g. The bandgap was determined as the intersection point between the energy axis and the line extrapolated from the linear portion of the absorption edge in a plot of the Kubelka–Munk function against the energy E.[14a,b] As shown in Figure S2 in the Supporting Information, the bandgaps of **1**–**6** are 3.30, 2.45, 2.17, 2.36, 2.48, and 2.64 eV, respectively, which suggest semiconductor characteristics. These bandgaps are relevant to the energy-level differences between the oxygen π-type HOMO and the tungsten π-type LUMO.[14c] Similar behaviors have been previously encountered in several reported organic–inorganic hybrid TMSPs, such as $[\{Ni_6(\mu_3\text{-}OH)_3(en)_2(H_2O)_8\}(B\text{-}\alpha\text{-}PW_9O_{34})\cdot 7\,H_2O$ ($E_g = 2.89$ eV),[4d] $[Co_2(bpy)_6\text{-}(W_6O_{19})_2]$ ($E_g = 2.20$ eV),[14d] and $[Ag_2(3atrz)_2]_2[HPMo^{VI}_{10}Mo^{V}_2O_{40}]$ ($E_g = 2.15$ eV, 3atrz = 3-amino-1,2,4-triazole).[14e] Comparison of the optical bandgaps of **1**–**6** reveals that the E_g values appear to be dependent on the structures of the POM-based cluster hybrids. That is, the band gaps change slightly for compounds with similar structures (**2**–**4** and **5**–**6**) while the bandgaps vary greatly when their structures (**1** and **2**–**6**) are somewhat different. Besides, the E_g values decrease with increasing dimensionality or complexity of the structures, as pointed out by Kanatzidis et al.[15] and Papavassiliou.[16]

Description of the structures

The experimental powder (P) XRD patterns of **1**–**6** are in good accordance with the simulated XRD patterns obtained from the single-crystal X-ray diffraction data, and suggest high phase purity of the samples (Figure S3 in the Supporting Information). The intensity differences between experimental and simulated XRD patterns may be ascribed to the variation in preferred orientation of the powder samples during collection of the experimental PXRD patterns. In addition, bond valence sum calculations[17] indicate that the oxidation states of W and Mn atoms in **1**–**6** are +6 and +2/+3, respectively. Considering the charge balance of **1**–**6**, some protons were added to their formulas. Additionally, in the description of crystal structures, the long Mn–O bonds are considered because of the evident Jahn–Teller distortion of Mn^{III} ions in the crystal field leading to the elongation of the Mn–O distances.[9a] Single-crystal X-ray diffraction showed that **1**, **2**, **3**, **4**, and **6** crystallize in the triclinic space group $P\bar{1}$, whereas **5** belongs to the monoclinic space group $P2_1/c$. The molecular structure of **1** consists of mixed-valent, Mn_6-cluster-encapsulating, dimeric POA $[(B\text{-}\alpha\text{-}SiW_9O_{34})_2Mn^{III}_4Mn^{II}_2O_4(H_2O)_4]^{12-}$ (**1a**), in which four active coordinated water molecules in the mixed-valent $[Mn^{III}_4Mn^{II}_2O_4(H_2O)_4]^{8+}$ cluster can be effectively replaced by two or four organic ligands to create a series of organic–inorganic hybrid species $[(B\text{-}\alpha\text{-}SiW_9O_{34})_2Mn^{III}_4Mn^{II}_2O_4(H_2O)_{4-n}(L)_n]^{12-}$ (**2**–**6**). In other words, the POA skeletons of **1**–**6** all are composed of two trivacant Keggin $[B\text{-}\alpha\text{-}SiW_9O_{34}]^{10-}$ fragments and a mixed-valent, hexa-Mn $\{Mn^{III}_4Mn^{II}_2O_4(H_2O)_{4-n}(L)_n\}$ cluster. Therefore, only the structure description of **1** is discussed herein in detail.

The fundamental structural unit of **1** comprises a dimeric sandwich-type POA $[(\text{B-}\alpha\text{-SiW}_9\text{O}_{34})_2\text{Mn}^{\text{III}}{}_4\text{Mn}^{\text{II}}{}_2\text{O}_4(\text{H}_2\text{O})_4]^{12-}$ (**1 a**), four discrete triprotonated $[\text{H}_3\text{deta}]^{3+}$ cations, and eight lattice water molecules. The **1 a** moiety(Figure 1 a) is constructed from two trivacant $[\text{B-}\alpha\text{-SiW}_9\text{O}_{34}]^{10-}$ fragments accommodating a mixed-valent hexa-Mn $[\text{Mn}^{\text{III}}{}_4\text{Mn}^{\text{II}}{}_2\text{O}_4(\text{H}_2\text{O})_4]^{8+}$ cluster, in which two head-to-head $[\text{B-}\alpha\text{-SiW}_9\text{O}_{34}]^{10-}$ fragments in the staggered fashion are linked by four Mn^{III} and two Mn^{II} ions through twelve μ_2-O atoms from lacunae of two $[\text{B-}\alpha\text{-SiW}_9\text{O}_{34}]^{10-}$ fragments, two μ_4-O atoms from two SiO_4 groups, two extraneous μ_3-O atoms, and two extraneous μ_4-O atoms, with formation of a sandwich-type structure. In each $[\text{B-}\alpha\text{-SiW}_9\text{O}_{34}]^{10-}$ fragment, the Si^{IV} center has a tetracoordinate distorted tetrahedral geometry defined by three μ_4-O atoms from three W_3O_{13} triads and a fourth μ_4-O atom linking to the central $[\text{Mn}^{\text{III}}{}_4\text{Mn}^{\text{II}}{}_2\text{O}_4(\text{H}_2\text{O})_4]^{8+}$ cluster core with Si–O distances of 1.594(14)–1.654(12) Å. The hexanuclear $[\text{Mn}^{\text{III}}{}_4\text{Mn}^{\text{II}}{}_2\text{O}_4(\text{H}_2\text{O})_4]^{8+}$ cluster in **1 a** has a C_i-symmetric, face-sharing, double-cubane geometry (Figure 1 b, c), and each cubane consists of three Mn^{III} and one Mn^{II} centers with two of the Mn^{III} centers shared by the other cubane. There are three crystallographically unique Mn ions in **1 a**, which all exhibit a distorted hexacoordinate octahedral geometry with different coordination environments. The octahedral Mn1^{III} ion is coordinated by two μ_2-O atoms from the lacunary sites of one $[\text{B-}\alpha\text{-SiW}_9\text{O}_{34}]^{10-}$ fragment (Mn^{III}–μ_2-O 1.881(14)–1.940(13) Å), one extraneous μ_3-O atom (Mn^{II}–μ_3-O 1.892(12) Å) and one extraneous μ_4-O atom (Mn^{III}–μ_4-O 1.877(14) Å) constituting the equatorial plane, and one μ_4-O atom from a SiO_4 group (Mn^{III}–μ_4-O 2.323(11) Å and one water O atom (Mn^{III}–O_w 2.342(14) Å) at two polar positions. The Mn2^{III} ion has an octahedral geometry in which the equatorial plane is built by two μ_2-O atoms from a $(\text{B-}\alpha\text{-SiW}_9\text{O}_{34})^{10-}$ fragment (Mn^{III}–μ_2-O 1.916 (12)–2.155(13) Å) and two extraneous μ_4-O atoms (Mn^{III}–μ_4-O 1.912(12)–2.413(12) Å), and the two polar positions are occupied by one μ_4-O atom from an SiO_4 group (Mn^{III}–μ_4-O 2.011(13) Å) and one extraneous μ_3-O atom (Mn^{III}–μ_3-O 1.855(13) Å). The octahedral coordination sphere of the Mn3^{II} ion is constituted by two μ_2-O atoms from a $(\text{B-}\alpha\text{-SiW}_9\text{O}_{34})^{10-}$ fragment (Mn^{II}–μ_2-O 2.061(15)–2.117(12) Å), one extraneous μ_3-O atom (Mn^{II}–μ_3-O 2.246(12) Å) and one extraneous μ_4-O atom (Mn^{II}–μ_4-O 2.155(14) Å) in the equatorial plane, and one μ_4-O atom from a SiO_4 group (Mn^{II}–μ_4-O 2.260(11) Å) and one water O atom (Mn^{II}–O_w 2.110(15) Å) in the two polar positions. This structure is somewhat akin to that of$\{[\text{X-W}_9\text{O}_{34}]_2[\text{Mn}^{\text{III}}{}_4\ \text{Mn}^{\text{II}}{}_2\text{O}_4(\text{H}_2\text{O})_4]\}^{12-}$ ($\text{X}=\text{Si}^{\text{IV}}$, Ge^{IV}) previously communicated by Cronin et al.[9a] There has been increasing interest in creating high-nuclearity Mn-substituted POMs containing polynuclear Mn^{III} ions, because these species can offer the essential ingredients of SMMs such as a large axial anisotropy arising from the existence of Jahn–Teller-distorted Mn^{III} ions.[18] To date, some progress has been made in the preparation of large MSPs including Mn^{III} ions from dinuclear to multinuclear aggregates by overcoming the obstacles that Mn^{III} ions are unstable in aqueous solution and tend to transform into Mn^{II} and Mn^{IV} ions.[9,19] For example, in 2007, Wang et al. isolated a mixed-valent, hexa-Mn, double-sandwich-type MSP based on two different lacunary POM building blocks, namely, $[\{\text{Mn}^{\text{II}}(\text{H}_2\text{O})\}_2\text{Mn}^{\text{III}}{}_4(\text{SiW}_6\text{O}_{26})\ (\text{SiW}_9\text{O}_{34})_2]^{16-}$, by a simple aqueous method.[19d] In 2011, Cronin and co-workers isolated another mixed-valent Mn_6-substituted trimeric MSP with three distinct lacunary POM building units, namely, $[\text{Mn}^{\text{III}}{}_2\text{Mn}^{\text{II}}{}_4(\mu_3\text{-O})_2(\text{H}_2\text{O})_4(\text{B-}\beta\text{-SiW}_8\text{O}_{31})(\text{B-}\beta\text{-SiW}_9\text{O}_{34})(\gamma\text{-SiW}_{10}\text{O}_{36})]^{18-}$.[19e] In 2009, Wang et al. reported tetradeca-Mn-substituted MSP $[(\text{Mn}^{\text{III}}{}_{13}\text{Mn}^{\text{II}}\text{O}_{12}\text{-}(\text{PO}_4)_4(\text{PW}_9\text{O}_{34})_4]^{31-}$, which is composed of two $[\text{Mn}_4\text{O}_3(\text{B-}\alpha\text{-PW}_9\text{O}_{34})]^{4-/3-}$ fragments and two $[\text{Mn}_3\text{O}_3(\text{B-}\alpha\text{-PW}_9\text{O}_{34})]^{6-}$ fragments connected by four $\text{PO}_4{}^{3-}$ linkers into a tetramer.[19g] In 2011, Fang and collaborators discovered two giant multi-Mn-substituted species, namely, the Mn_{14}-based isopolytungstate $[\{\text{Mn}^{\text{III}}{}_3\text{Mn}^{\text{IV}}{}_4\text{O}_4(\text{OH})_2(\text{OH}_2)\}_2(\text{W}_6\text{O}_{22})(\text{H}_2\text{W}_8\text{O}_{32})_2\ (\text{H}_4\text{W}_{13}\text{O}_{46})_2]^{26-}$ containing three types of iso-POM building blocks[19i] and the core–shell cluster aggregate $[(\text{P}_8\text{W}_{48}\text{O}_{184})\{(\text{P}_2\text{W}_{14}\text{Mn}_4\text{O}_{60})\text{-}(\text{P}_2\text{W}_{15}\text{Mn}_3\text{O}_{58})_2\}_4]^{144-}$ constructed from 16 corner-sharing Dawson-type units.[19j] Nevertheless, only four examples of POM-based complexes with mixed-valent Mn clusters ($\{\text{Mn}^{\text{III}}{}_4\text{Mn}^{\text{II}}{}_2\}$, $\{\text{Mn}^{\text{III}}{}_3\text{Mn}^{\text{IV}}\}$, $\{\text{Mn}^{\text{III}}{}_6\text{Mn}^{\text{IV}}\}$, and $\{\text{Mn}^{\text{IV}}{}_2\text{Mn}^{\text{III}}{}_6\text{Mn}^{\text{II}}{}_4\}$) exhibiting SMM behavior have been reported hitherto.[2c,9] In 2008, Cronin et al. reported the first $\text{Mn}^{\text{II/III}}$-based SMM $\{[\text{XW}_9\text{O}_{34}]_2[\text{Mn}^{\text{III}}{}_4\text{Mn}^{\text{II}}{}_2\text{O}_4(\text{H}_2\text{O})_4]\}^{12-}$ ($\text{X}=\text{Si}^{\text{IV}}$, Ge^{IV}), made up of two $[\text{XW}_9\text{O}_{34}]^{10-}$ segments sandwiching a mixed-valent, hexanuclear $[\text{Mn}^{\text{III}}{}_4\text{Mn}^{\text{II}}{}_2\text{O}_4(\text{H}_2\text{O})_4]^{8+}$ cluster.[9a] Later, Fang et al. obtained two organic–inorganic hybrid, tetra-Mn-substituted monomers with SMM behavior, namely, $[(\alpha\text{-P}_2\text{W}_{15}\text{O}_{56})\text{-Mn}^{\text{III}}{}_3\text{Mn}^{\text{IV}}\text{O}_3(\text{CH}_3\text{COO})_3]^{8-}$[9b] and $[(\text{A-}\beta\text{-SiW}_9\text{O}_{34})\text{Mn}^{\text{III}}{}_3\text{Mn}^{\text{IV}}\text{O}_3\text{-}(\text{CH}_3\text{COO})_3]^{6-}$,[9d] by grafting a distorted cubane $[\text{Mn}_4\text{O}_4(\eta^2{:}\mu_2\text{-CH}_3\text{COO})_3]^{2+}$ cluster to the lacunary site of $[\alpha\text{-P}_2\text{W}_{15}\text{O}_{56}]^{12-}$ and $[\text{A-}\beta\text{-SiW}_9\text{O}_{34}]^{10-}$ POAs, and hepta-Mn-inserted SMM $[(\alpha\text{-P}_2\text{W}_{15}\text{O}_{56})_2\text{Mn}^{\text{III}}{}_6\text{Mn}^{\text{IV}}\text{O}_6(\text{H}_2\text{O})_6]^{14-}$.[9c] Recently, Wang et al. made a new cluster exhibiting three different oxidation states, namely, $\{[\text{Mn}^{\text{IV}}{}_2\ \text{Mn}^{\text{III}}{}_6\text{Mn}^{\text{II}}{}_4(\mu_3\text{-O})_6(\mu\text{-OH})_4(\text{H}_2\text{O})_2(\text{CO}_3)_6][\text{B-}\beta\text{-SiW}_6\text{O}_{26}]_2\}^{18-}$, which has the highest known Mn nuclearity in the POM-based SMM family.[2c] These previous achievements not only demonstrate the great potential for constructing

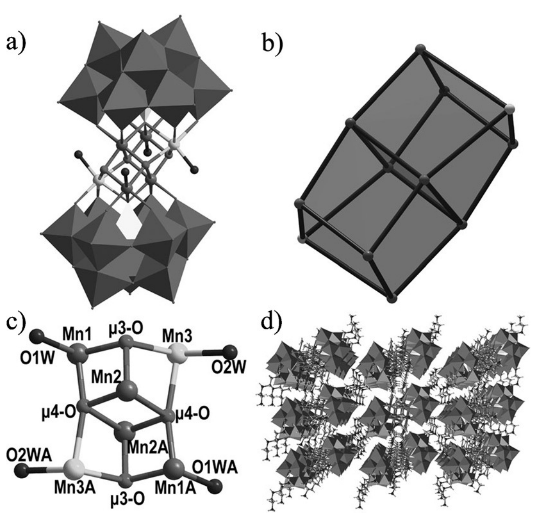

Figure 1. a) Polyhedral/ball-and-stick representation of **1 a**. b) The face-sharing double-cubane core in **1 a**. c) The connection motif of the $[\text{Mn}^{\text{III}}{}_4\text{Mn}^{\text{II}}{}_2\text{O}_4(\text{H}_2\text{O})_4]^{8+}$ cluster core in **1 a**. d) 3D supramolecular framework of **1** along the *a* axis. Mn^{III} large dark, Mn^{II} large light, O small gray, H_2O small dark. All isolated H_2O molecules are omitted for clarity.

© 2016 Wiley-VCH Verlag GmbH & Co. KGaA, Weinheim

SMMs of mixed-valent MSPs, but also attract and motivate more chemists to develop and investigate this domain of POM-based SMM materials.

The design and construction of metal-containing supramolecular networks have attracted increasing attention in the fields of crystal engineering and supramolecular chemistry, since they can provide neoteric topologies and functional materials.[20] Moreover, POM-based supramolecular architectures are among the most promising materials in the fields of chemicobiology, materials chemistry, and so on.[21] In this respect, 3D supramolecular structures also exist in **1**–**6**. In the structure of **1**, the N atoms of deta ligands functioning as proton donors participate in the formation of N–H···O interactions with the surface O atoms of $[B\text{-}\alpha\text{-}SiW_9O_{34}]^{10-}$ fragments serving as proton acceptors. Specifically, adjacent **1a** units are interconnected by N–H···O interactions with amino groups of free deta ligands to form a 1D supramolecular chain along the *a* axis (Figure S4 in the Supporting Information). Furthermore, neighboring chains are connected with each other to give a 3D supramolecular framework (Figure 1 d), in which each **1a** unit acts as a ten-connected node. Topological analysis of this net was performed with a Schläfli symbol of $\{4^4{\cdot}6^{16}{\cdot}8^{17}{\cdot}10^8\}$ by using TOPOS 4.0 (Figure 2 a).

Compound **2** consists of a dimeric $[(B\text{-}\alpha\text{-}SiW_9O_{34})_2Mn^{III}_4Mn^{II}_2O_4(H_2O)_2(Hen)_2]^{10-}$ (**2a**) unit (Figure 3 a), five discrete diprotonated $[H_2en]^{2+}$ cations, and eight water molecules of crystallization. The structure of **2a** can be viewed as a derivative of **1a** with two coordinated water molecules replaced by two en ligands (Mn–N: 2.283(9) Å; Figure 3 c). Although similar hexa-Mn-substituted, trivacant Keggin POMs $\{[XW_9O_{34}]_2[Mn^{III}_4Mn^{II}_2O_4(H_2O)_4]\}^{12-}$ (X = Si^{IV}, Ge^{IV}) (**A** and **B**)[9a] were reported, to the best of our knowledge, organic–inorganic hybrid, hexa-Mn-sandwiched, trivacant Keggin-type POMs **2**–**6** are addressed here for the first time. In comparison with **2**, three obvious distinctions can be summarized: 1) **2** was made by the synergetic reaction of trivacant precursor $[A\text{-}\alpha\text{-}SiW_9O_{34}]^{10-}$ with the Mn^{2+} cation in the presence of apm and en, whereas **A** and **B** were prepared by using divacant Keggin precursors, which transformed into trivacant POM units in the reaction procedure; 2) from the viewpoint of synthetic technique, **2** was hydrothermally made at 90 °C, whereas **A** and **B** were obtained at 50 °C in conventional aqueous solution, which also indicates that the hydrothermal method is an effective strategy for producing novel organic–inorganic hybrid POMs; 3) en ligands were introduced into the central $\{Mn^{III}_4Mn^{II}_2O_4(H_2O)_4\}$ cluster core through the coordination of N atoms with Mn^{III} centers in **2**, but not in **A** and **B**.

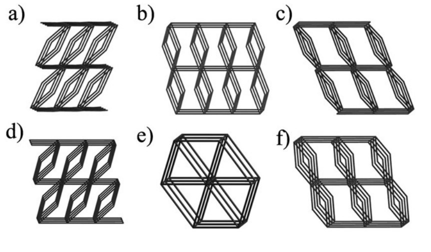

Figure 2. a–f) The 3D supramolecular topology along the *b*, *a*, *a*, *b*, *a*, and *b* axes of **1**–**6**, respectively. Black: $[(SiW_9O_{34})_2Mn^{III}_4Mn^{II}_2O_4]$ nodes; gray: organic amine nodes.

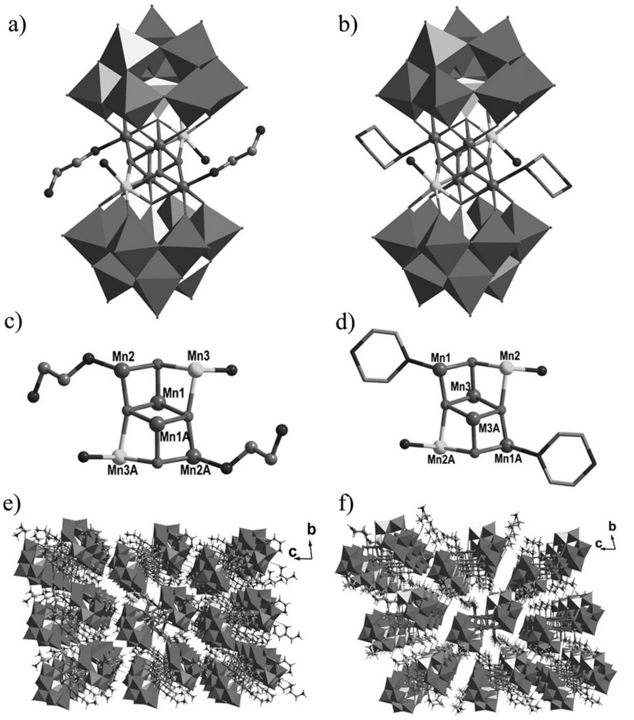

Figure 3. a–b) Polyhedral/ball-and-stick representation of **2a** and **3a**. c), d) Connection motifs of the $\{Mn^{III}_4Mn^{II}_2O_4(H_2O)_2(Hen)_2\}$ and $\{Mn^{III}_4Mn^{II}_2O_4(H_2O)_2(ppz)_2\}$ clusters in **2a** and **3a**. e) 3D supramolecular framework of **2** and **3** along the *a* axis. Mn^{III} large dark, Mn^{II} large light, O small gray, H_2O small dark, N dark, C gray. All isolated H_2O molecules are omitted for clarity.

In addition, neighboring **2a** units are linked to coordinated water molecules by O–H···O interactions (O···O 2.728(10) Å, Figure S5 in the Supporting Information) to form a 1D supramolecular chain along the *c* axis. Moreover, the 1D supramolecular chains are further connected together through N–H···O interactions between free diprotonated $[H_2en]^{2+}$ cations and **2a** units to form a 3D supramolecular framework (Figure 2 e), in which each **2a** unit acts as a eight-connected node, with a Schläfli symbol of $\{4^2{\cdot}6^{12}{\cdot}8^9{\cdot}10^5\}$ (Figure 2 b).

The molecular structure of **3** is composed of an organic–inorganic hybrid $[(B\text{-}\alpha\text{-}SiW_9O_{34})_2Mn^{III}_4Mn^{II}_2O_4(H_2O)_2(ppz)_2]^{12-}$ (**3a**) dimeric unit (Figure 3 b), four diprotonated $[H_2ppz]^{2+}$ cations, two diprotonated $[H_21,3\text{-}dap]^{2+}$ cations, and six lattice water molecules. The $\{Mn^{III}_4Mn^{II}_2O_4(H_2O)_2\}$ unit is associated with two attached ppz ligands through N atoms (Figure 3 d) to give a hybrid that can be regarded as the result of two ppz ligands substituting for two en ligands in **2a**. In addition, **4a** is the same as **3a**, and hence it is not described here. Moreover, discrete **3a** units are regularly distributed (Figure 3 f). Figure S6 in the Supporting Information shows that neighboring **3a** units are closely aligned in an orderly arrangement, and thus it can be conjectured that the ppz ligands grafted onto two sides of the $\{Mn^{III}_4Mn^{II}_2O_4\}$ unit can to some degree decrease the steric hindrance and favor the closest packing of **3a** units. For each ppz ligand, only one N atom is involved in the N–H···O interactions with the O atoms of both **3a** and lattice water molecules. As a result, the combination of proton donors from free and coordinated ppz ligands with proton acceptors from O atoms of [B-α-SiW$_9$O$_{34}$]$^{10-}$ fragments, lattice water molecules (N–H···O 2.85(5)–3.18(3) Å, O–H···O 2.77(1) Å) results in a 3D supramolecular structure (Figure 3 f) in which each **3a** unit acts as an eight-connected node with a Schläfli symbol of {4^6·6^{18}·10^4} (Figure 2 c).

Single-crystal X-ray diffraction revealed that **5** crystallizes in the monoclinic space group $P2_1/c$, and **6** in the triclinic space group $P\bar{1}$. In contrast to **1**–**4**, the POA skeletons of both **5** and **6** consist of a Mn$_6$-substituted units (Figure 4 a): [(B-α-SiW$_9$O$_{34}$)$_2$Mn$^{III}_4$Mn$^{II}_2$O$_4$(ppz)$_4$]$^{12-}$ (**5a**) and [(B-α-SiW$_9$O$_{34}$)$_2$Mn$^{III}_4$Mn$^{II}_2$O$_4$(Hppz)$_4$]$^{8-}$ (**6a**). The four aqua ligands in the {Mn$^{III}_4$Mn$^{II}_2$O$_4$(H$_2$O)$_4$} unit are totally replaced by ppz ligands in **5a** and **6a**, which is the biggest difference between **5a**/**6a** and **1a**–**4a** (Figure S7 in the Supporting Information). The substitution of aqua ligands by en groups has been observed in Ni$_6$ systems,[11a,20] but not in Mn$_6$ systems. Furthermore, **5** also exhibits a 3D supramolecular structure due to H-bonding interactions among **5a** units and organic ligands. A remarkable structural feature of **5** is the existence of three kinds of hydrogen bonds. One involves the coordinated ppz groups of [Mn$^{III}_4$Mn$^{II}_2$ O$_4$(ppz)$_4$]$^{8+}$ clusters as donors and the O atoms of [B-α-SiW$_9$O$_{34}$]$^{10-}$ fragments as acceptors with an N···O distance of 2.792(8) Å (Figure S8 in the Supporting Information). Another involves the free ppz groups with a distance of 3.068(9) Å. These two kinds of hydrogen bonds contribute to the formation of a 2D supramolecular layer in **5** (Figure S9 in the Supporting Information). The third type exists between **5a** units and free [H$_3$deta]$^{3+}$ cations, and results in the construction of the 3D supramolecular structure (Figure 4 c) with a Schläfli symbol of {3^6·4^6·5^3·6^{12}·10}, in which each **5a** unit acts as an eight-connected node. Compound **6** exhibits a novel 3D supramolecular framework with a Schläfli symbol of {4^6·6^{18}·10^4} (Figure 2 f), in which each {Mn$_6$Si$_2$W$_{18}$} unit acts as an eight-connected node. In contrast to **2**–**4**, the introduction of more ppz ligands is propitious to the stabilization of the 3-D supramolecular frameworks.

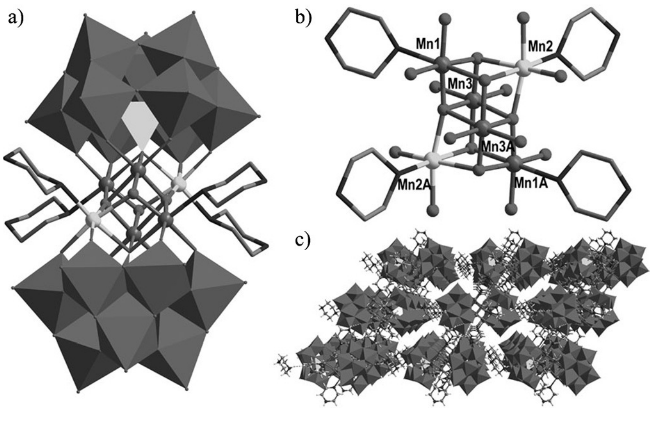

Figure 4. a) Polyhedral/ball-and-stick representation of **5a** and **6a**. b) The connection motif of the {Mn$^{III}_4$Mn$^{II}_2$O$_4$(ppz)$_4$} cluster in **5a**. c) 3D supramolecular framework of **5** along the b axis. Mn^{III} large dark, Mn^{II} large light, O small gray, H$_2$O small dark, N dark, C gray. All isolated H$_2$O molecules are omitted for clarity.

Magnetic properties

SMMs, that is, compounds exhibiting slow relaxation of magnetization below a blocking temperature, have witnessed great development in recent years due to their unique properties and potential applications in high-density magnetic information storage and computation devices,[22] since the discovery of SMM behavior in TM coordination clusters two decades ago.[6] Lacunary POMs, as a kind of highly charged inorganic anionic ligands with confined ligation environments and rich redox properties, are good candidates for incorporating unusual TM magnetic clusters into their skeletons through μ-oxo/hydroxo groups to create novel POM-based SMMs. Moreover, nonmagnetic POM frameworks insure effective magnetic isolation of TM clusters generated in situ from each other, so that intermolecular interactions are usually negligible. This offers a good opportunity for probing magnetic exchange interactions and electron delocalization in highly symmetrical clusters. Studies on SMMs are mainly focused on polynuclear metal clusters, largely owing to their intrinsic magnetic characteristics, such as high-spin ground state and magnetocrystalline anisotropy, which lead to a spin-reversal barrier for slow relaxation of magnetization. Despite a continuous stream of SMMs featuring diverse metal ions and nuclearities, the exploration of MSP-based SMMs is still in its infancy.[2c,9,23] The d^4 Mn^{III} ion has an ^{5}E$_g$ ground state in a hexacoordinate octahedral environment, and splitting of the ^{5}E$_g$ ground state into ^{5}A$_{1g}$ and ^{5}B$_{1g}$ can be induced by the Jahn–Teller effect, corresponding to an elongated axis with the zero-field splitting parameter $D<0$ in most instances, or a compressed axis along with $D>0$ in rare cases,[24] which make Mn^{III} ions particularly popular for constructing SMMs, as is confirmed by the fact that nearly all SMMs in POM chemistry and even coordination chemistry contain Mn^{III} ions.[25] Therefore, research on novel Mn^{III} SMMs remains a long-standing challenge.

As **1**–**6** contain the similar {Mn$^{III}_4$Mn$^{II}_2$} cores, only the magnetic properties of **3** and **6** are discussed here. The plots of χ_M and $\chi_M T$ versus T of **3** and **6** in a constant field of 1000 Oe in the temperature range of 1.8–300 K are illustrated in Figure S10a of the Supporting Information and Figure 5 a. The χ_M value shows a moderate increase from 0.061 emu K mol^{-1} at 300 K to 0.847 emu K mol^{-1} for **3** and 0.803 emu K mol^{-1} for **6** at 20 K and then exponentially reaches maxima of 13.43 emu K mol^{-1} for **3** and 12.42 emu K mol^{-1} for **6** at 1.8 K. Correspondingly, the $\chi_M T$ values of 18.23 emu K mol^{-1} at 300 K for **3** and 18.15 emu K mol^{-1} at 300 K for **6** are slightly smaller than the excepted value (20.75 emu K mol^{-1}, $g=2$) for four noninteracting Mn^{III} ($S=2$) and two noninteracting Mn^{II} ($S=5/2$) ions. On cooling, the $\chi_M T$ value diminishes gradually from 18.23 emu K mol^{-1} at 300 K to a minimum of 13.38 emu K mol^{-1} at 70 K for **3** and from 18.15 emu K mol^{-1} at 300 K to a minimum of 13.11 emu K mol^{-1} at 85 K for **6**. Below 70 K for **3** and 85 K for **6**, the $\chi_M T$ value increases rapidly and reaches a maximum of 24.39 emu K mol^{-1} at 4 K for **3** and 22.47 emu K mol^{-1} at 3 K for

© 2016 Wiley-VCH Verlag GmbH & Co. KGaA, Weinheim

6 and then decreases sharply to 24.17 emu K mol^{-1} for **3** and 22.34 emu K mol^{-1} for **6** at 1.8 K. Such behavior indicates the coexistence of both antiferromagnetic Mn^{II}–Mn^{III} coupling and ferromagnetic Mn^{III}–Mn^{III} coupling. The final decrease can be attributed to the zero-field splitting of the Mn^{III} centers and the Zeeman effect of the applied field. The magnetic data between 127 and 300 K for **3** and between 120 and 300 K for **6** conforms to the Curie–Weiss law, with a Curie constant of $C=23.17$ emu K mol^{-1} and Weiss constant of $\theta=-86.72$ K for **3** (Figure S11 in the Supporting Information) and $C=24.08$ emu K mol^{-1} and $\theta=-104.03$ K for **6** (Figure S12 in the Supporting Information), which indicate dominant antiferromagnetic exchange interactions. In comparison with the magnetic properties of $(C_4H_{10}NO)_{12}\{[SiW_9O_{34}]_2[Mn^{III}_4Mn^{II}_2O_4(H_2O)_4]\}\cdot 15H_2O$ reported in Ref. [9a], although there are some differences in the magnetic data for **3** and **6**, their magnetic behaviors are still similar and they all show dominant antiferromagnetic coupling interactions. Clearly, the gradual replacement of the coordinated water molecules in the $[Mn^{III}_4Mn^{II}_2O_4(H_2O)_4]^{8+}$ cluster by organic groups results in changes of the Mn−O distances and Mn-O-Mn angles, and further gives rise to the small changes of their magnetic data.

To confirm the magnitude of the spin ground state, variable-field magnetization data were collected for **3** and **6** in the range of 0–7 T at 2 K, and the plots of reduced magnetization $M/N\beta$ versus H are shown in Figure S10b of the Supporting Information and Figure 5b. The magnetization increases abruptly to reach approximately 7.7 $N\beta$ for **3** and 7.9 $N\beta$ for **6** at 0.8 T and continues increasing in a linear fashion to reach 10.3 $N\beta$ for **3** and 9.9 $N\beta$ for **6** at 7 T with the appearance of the saturation value. The magnetizations of 10.3 $N\beta$ for **3** and 9.9 $N\beta$ for **6** at 7 T suggests a ground spin state of $S=5$, from which it can be deduced that the spins of two Mn^{II} atoms and two Mn^{III} atoms are parallel and the spins of two Mn^{III} atoms are antiparallel.

In addition, comparing bond lengths and bond angles reveals that the distances between Mn^{III} and Mn^{II} atoms in **1**–**6** are similar to those of **A** (Table S1 in the Supporting Information). We speculate that they have similar magnetic behaviors. Thus, besides these static magnetic susceptibility data, the dynamic properties of **3** and **6** were also studied by means of frequency-dependent ac susceptibility measurements in the temperature range of 1.8–10 K to probe whether they exhibit SMM characteristics. The frequency dependence of both in-phase (χ'_M) and out-of-phase (χ''_M) components were observed in an applied dc field of zero (Figure S10 c,d of the Supporting Information, Figure 5 c,d), which is a clear indication of slow relaxation of magnetization. Moreover, it is evident that well-resolved peaks of the χ'_M and χ''_M signals emerge in the frequency range of 100–999 and 999 Hz for **3** and 32–999 and 316–

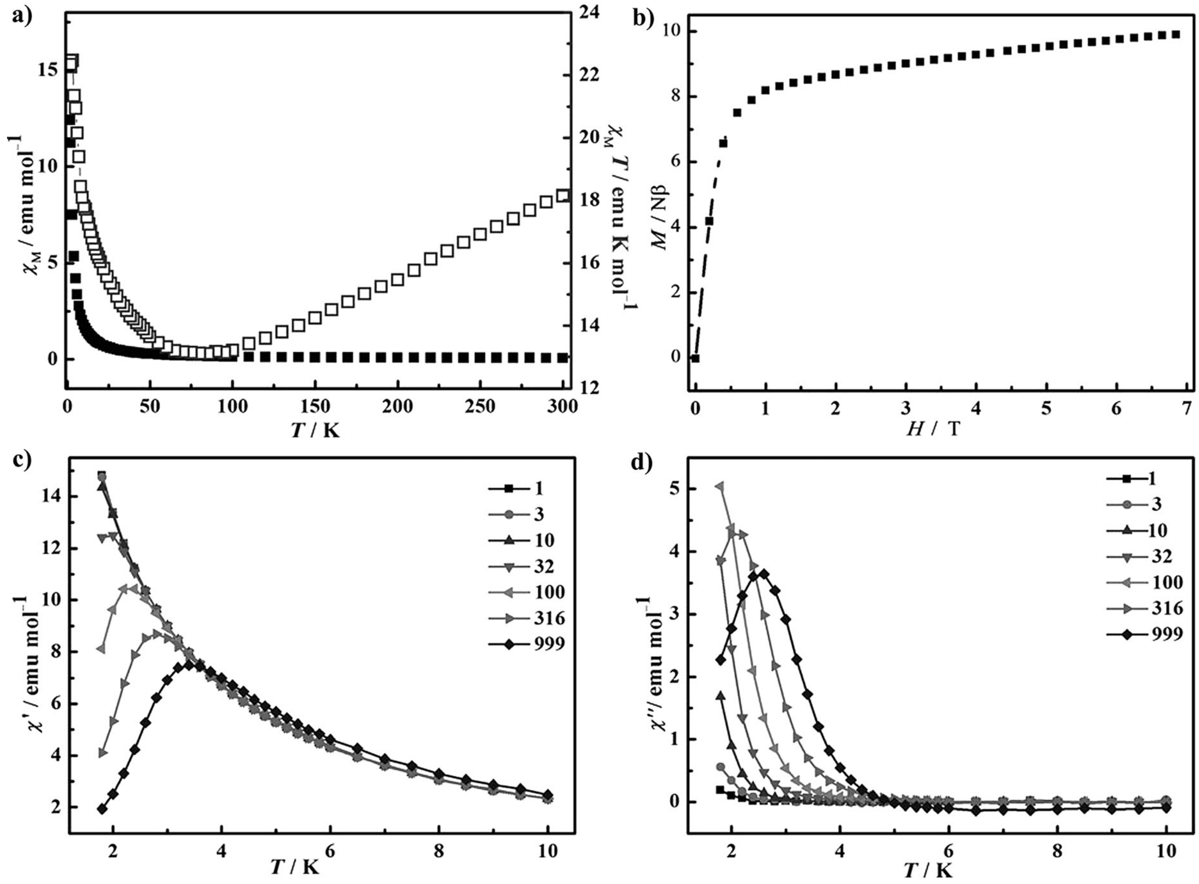

Figure 5. a) Temperature dependence of the molar magnetic susceptibility χ_M and the product of the molar magnetic susceptibility and temperature $\chi_M T$ for **6** between 1.8 and 300 K. b) Magnetization versus field for **6** at 2 K. c) Variable-temperature in-phase (χ') ac susceptibilities at various frequencies for **6** in zero dc field. d) Variable-temperature out-of-phase (χ'') ac susceptibilities at various frequencies for **6** in zero dc field.

© 2016 Wiley-VCH Verlag GmbH & Co. KGaA, Weinheim

999 Hz for **6**, respectively, which strongly indicate SMM behavior of **3** and **6**. Actually, SMMs showing field-reduced slow relaxation of the magnetization have been already observed in Mn^{III} complexes such as the Mn^{III}-salen-type compound $[Mn^{III}$(5-TMAM(*R*)-salmen)$(H_2O)Co^{III}(CN)_6]\cdot 7\,H_2O\cdot MeCN$ [5-TMAM-(*R*)-salmen = (*R*)-*N*,*N*′-(1-methylethylene)bis(5-trimethylammoniomethylsalicylideneiminate][25a] and the mononuclear octahedral Mn^{III} complex $[Mn(dbm)_2(L)_2](ClO_4)$ (dbm = dibenzoylmethanido, L = pyridine),[25c] whereas this behavior is rare in POMs, and was only encountered in $[Ln(W_5O_{18})_2]^{9-}$,[8b] $\{[XW_9O_{34}]_2[Mn^{III}{}_4Mn^{II}{}_2O_4(H_2O)_4]\}^{12-}$ (X = Si^{IV}, Ge^{IV}),[9a] and $[M(SiW_9O_{34})_2]^{17/18-}$ (M = Fe^{III}, Co^{II}, Mn^{III}).[23]

Thermogravimetric analysis (TGA)

To investigate the thermal stability of **1**–**6**, TGA was carried out in flowing air at a heating rate of 10 °C min^{-1} in the temperature range of 30–800 °C. As shown in Figure S13 in the Supporting Information, the TG curve of **1** displays one-step slow weight loss in the range of 30–800 °C. The total weight loss of 14.15 % is assigned to the release of eight lattice water molecules, four coordinated water molecules, the removal of four free deta ligands, and the loss of twelve protons (calcd 13.43 %). The weight loss process of **2** is divided into two steps in the range of 30–800 °C. The weight loss of 9.86 % in the range of 30–602 °C corresponds to the release of eight lattice water molecules, two coordinated water molecules, five free en ligands, and one coordinated en ligand (calcd 9.90 %). Above 602 °C a gradual weight loss of 2.92 % up to 800 °C is observed and assigned to the removal of the remaining one coordinated en ligand and the loss of twelve protons (calcd 3.08 %). The TG curve of **3** shows three weight-loss steps. In the range of 30–185 °C, the weight loss of 2.19 % is due to the loss of six lattice water molecules (calcd 1.91 %), and the weight loss of 11.06 % from 185 to 572 °C is approximately attributable to the removal of four free ppz ligands, two free 1,3-dap ligands, two coordinated water molecules, and one coordinated ppz ligand (calcd 10.85 %). The third weight loss of 3.61 % between 506 and 800 °C is assigned to the removal of the remaining one coordinated ppz ligand and the loss of twelve protons (calcd 3.43 %). The TG process of **4** displays one-step continuous weight loss in the range of 30–800 °C. The total weight loss of 14.72 % is assigned to the release of eight lattice water molecules, two coordinated water molecules, four free ppz ligands, two coordinated ppz ligands, and the loss of twelve protons (calcd 14.49 %). The TG curve of **5** displays two continuous stages of weight loss in the range of 30–800 °C. The first weight loss of 12.95 % from 30 to 295 °C is assigned to the release of twelve lattice water molecules, three free ppz ligands, two free deta ligands, and one coordinated ppz ligand (calcd 13.04 %).The second weight loss of 6.25 % between 295 and 800 °C is assigned to the decomposition of the remaining three coordinated ppz ligands and the loss of twelve protons (calcd 6.23 %). The TG curve of **6** displays two major weight loss stages in the range of 30–800 °C. The first weight loss of 10.47 % from 30 to 300 °C is attributable to the release of ten lattice water molecules, two free ppz ligands, two free en molecules, and one coordinated ppz ligand (calcd 10.79 %). The second weight loss of 6.76 % between 300 and 800 °C is approximately attributable to the removal of three coordinated ppz molecules and the loss of twelve protons (calcd 6.39 %). The observed experimental values are approximately consistent with the theoretical values.

Conclusion

Two different-sized and flexible organic N ligands were successfully grafted onto the surface of $\{Mn^{III}{}_4Mn^{II}{}_2O_4\}$ units to form organic covalently functionalized TMSPs **1**–**6** under hydrothermal conditions, which were characterized by elemental analysis, IR spectroscopy, TGA, and single-crystal X-ray crystallography. Furthermore, the successful isolation of **1**–**6** not only indicates that double-cubane $\{Mn^{III}{}_4Mn^{II}{}_2O_4(H_2O)_{4-n}(L)_n\}$ clusters are very stable in both conventional aqueous solution and hydrothermal systems, but also demonstrate that the hydrothermal technique can act as an effective approach for making novel mixed-valent TM-cluster-substituted POMs by combination of lacunary Keggin precursors with TM cations with a tunable role of organic ligands. Structural analyses indicate that the organic N ligands can substitute coordinated water molecules located on the outer positions of the $[Mn^{III}{}_4Mn^{II}{}_2O_4(H_2O)_4]^{8+}$ cores. As a consequence, further work based on the following aspects is in progress: 1) replacing four terminal water ligands of $[(B\text{-}\alpha\text{-}SiW_9O_{34})Mn^{III}{}_4Mn^{II}{}_2O_2(H_2O)_2]$ by multifunctional carboxylic ligands to make cluster–organic cages/chains/networks/frameworks, and 2) introducing other multilacunary POM precursors such as $[\alpha\text{-}P_2W_{15}O_{56}]^{12-}$,[26] $[P_6W_{18}O_{79}]^{20-}$,[27a] $[As_2W_{19}O_{67}(H_2O)]^{14-}$,[27b] $[As_4W_{40}O_{140}]^{28-}$,[27c] and $[Sb_2W_{22}O_{74}(OH)_2]^{12-}$[27d] to react with various TM or lanthanide ions to prepare novel metal-substituted POMs with interesting magnetic properties.

Acknowledgements

This work was supported by the NSFC (nos. 21571016, 91122028, and 21171030) and the NSFC for Distinguished Young Scholars (no. 20725101).

Keywords: cluster compounds · hydrothermal synthesis · manganese · mixed-valent compounds · polyoxometalates

[1] a) A. Dolbecq, E. Dumas, C. R. Mayer, P. Mialane, *Chem. Rev.* **2010**, *110*, 6009 – 6048; b) H. N. Miras, L. Vilà-Nadal, L. Cronin, *Chem. Soc. Rev.* **2014**, *43*, 5679 – 5699; c) C. L. Hill, C. M. Prosser-McCartha, *Coord. Chem. Rev.* **1995**, *143*, 407 – 455; d) H. Wang, S. Hamanaka, Y. Nishimoto, S. Irle, T. Yokoyama, H. Yoshikawa, K. Awaga, *J. Am. Chem. Soc.* **2012**, *134*, 4918 – 4924; e) M. Sadakane, E. Steckhan, *Chem. Rev.* **1998**, *98*, 219 – 238.

[2] a) F. Hussain, R. W. Gable, M. Speldrich, P. Kgerler, C. Boskovic, *Chem. Commun.* **2009**, 328 – 330; b) Y. F. Song, R. Tsunashima, *Chem. Soc. Rev.* **2012**, *41*, 7384 – 7402; c) Z. M. Zhang, S. Yao, Y. G. Li, Z. M. Su, E. B. Wang, *Chem. Commun.* **2013**, *49*, 2515 – 2517; d) H. Miao, X. Xu, Y. Xu, *Inorg. Chem.* **2014**, *53*, 2757 – 2759.

[3] a) I. V. Kozhevnikov, *Chem. Rev.* **1998**, *98*, 171 – 198; b) C. L. Hill, *J. Mol. Catal. A* **2007**, *262*, 2 – 6; c) S. S. Wang, G. Yu Yang, *Chem. Rev.* **2015**, *115*, 4893 – 4962.

[4] a) G. J. Cao, J. D. Liu, S. T. Zheng, *Chem. Commun.* **2015**, *51*, 2048 – 2051; b) X. X. Li, W. H. Fang, J. W. Zhao, G. Y. Yang, *Chem. Eur. J.* **2015**, *21*,

© 2016 Wiley-VCH Verlag GmbH & Co. KGaA, Weinheim

2315–2318; c) X. J. Sang, L. C. Zhang, W. L. Chen, E. B. Wang, *Chem. Commun.* **2014**, *50*, 14678–14681; d) J. W. Zhao, J. Zhang, S. T. Zheng, G. Y. Yang, *Chem. Eur. J.* **2007**, *13*, 10030–10045; e) J. M. Clemente-Juan, E. Coronado, *Coord. Chem. Rev.* **1999**, *193–195*, 361–394; f) J. M. Clemente-Juan, E. Coronade, A. Forment-Aliaga, J. R. Galán-Mascarós, C. Giménez-Saiz, C. J. Gómez-García, *Inorg. Chem.* **2004**, *43*, 2689–2694.

[5] a) A. J. Tasiopoulos, A. Vinslava, W. Wernsdorfer, K. A. Abboud, G. Christou, *Angew. Chem. Int. Ed.* **2004**, *43*, 2117–2121; *Angew. Chem.* **2004**, *116*, 2169–2173; b) P. Gerbier, N. Domingo, J. Gémez-Segura, D. Ruiz-Molina, D. B. Amabilino, J. Tejada, B. E. Williamson, J. Veciana, *J. Mater. Chem.* **2004**, *14*, 2455–2460; c) S. K. Langley, R. A. Stott, N. F. Chilton, B. Moubaraki, K. S. Murray, *Chem. Commun.* **2011**, *47*, 6281–6283; d) T. Lis, *Acta Crystallogr. Sect. B* **1980**, *36*, 2042–2045; e) M. Manoli, R. Inglis, M. J. Manos, V. Nastopoulos, W. Wernsdorfer, E. K. Brechin, A. J. Tasiopoulos, *Angew. Chem. Int. Ed.* **2011**, *50*, 4441–4444; *Angew. Chem.* **2011**, *123*, 4533–4536; f) A. J. Tasiopoulos, S. P. Perlepes, *Dalton Trans.* **2008**, 5537–5543.

[6] R. Sessoli, D. Gatteschi, A. Caneschi, M. A. Novak, *Nature* **1993**, *365*, 141–143.

[7] a) E. Coronado, J. R. Galán-Mascarós, C. J. Gómez-García, V. Laukhin, *Nature* **2000**, *408*, 447–449; b) E. Coronado, C. Giménez-Saiz, C. J. Gómez-García, *Coord. Chem. Rev.* **2005**, *249*, 1776–1796; c) X. K. Fang, P. Kögerler, *Chem. Commun.* **2008**, 3396–3398; d) U. Kortz, A. Müller, J. van Slageren, J. Schnack, N. S. Dalal, M. Dressel, *Coord. Chem. Rev.* **2009**, *253*, 2315–2327.

[8] a) M. Ibrahim, Y. H. Lan, B. S. Bassil, Y. X. Xiang, A. Suchopar, A. K. Powell, U. Kortz, *Angew. Chem. Int. Ed.* **2011**, *50*, 4708–4711; *Angew. Chem.* **2011**, *123*, 4805–4808; b) M. A. AlDamen, J. M. Clemente-Juan, E. Coronado, C. Martí-Gastaldo, A. Gaita-Arinõ, *J. Am. Chem. Soc.* **2008**, *130*, 8874–8875; c) J.-D. Compain, P. Mialane, A. Dolbecq, I. M. Mbomekallé, J. Marrot, F. Sécheresse, E. Rivière, G. Rogez, W. Wernsdorfer, *Angew. Chem. Int. Ed.* **2009**, *48*, 3077–3081; *Angew. Chem.* **2009**, *121*, 3123–3127; d) H. E. Moll, A. Dolbecq, J. Marrot, G. Rousseau, M. Haouas, F. Taulelle, G. Rogez, W. Wernsdorfer, B. Keita, P. Mialane, *Chem. Eur. J.* **2012**, *18*, 3845–3849; e) C. Ritchie, M. Speldrich, R. W. Gable, L. Sorace, P. Kögerler, C. Boskovic, *Inorg. Chem.* **2011**, *50*, 7004–7009; f) C. Lydon, M. M. Sabi, M. D. Symes, D. L. Long, M. Murrie, S. Yoshii, H. Nojiri, L. Cronin, *Chem. Commun.* **2012**, *48*, 9819–9826.

[9] a) C. Ritchie, A. Ferguson, H. Nojiri, H. N. Miras, Y. F. Song, D. L. Long, E. Burkholder, M. Murrie, P. Kögerler, E. K. Brechin, L. Cronin, *Angew. Chem. Int. Ed.* **2008**, *47*, 5609–5612; *Angew. Chem.* **2008**, *120*, 5691–5694; b) X. K. Fang, M. Speldrich, H. Schilder, R. Cao, K. P. O'Halloran, C. L. Hill, P. Kögerler, *Chem. Commun.* **2010**, *46*, 2760–2761; c) X. K. Fang, P. Kögerler, M. Speldrich, H. Schilder, M. Luban, *Chem. Commun.* **2012**, *48*, 1218–1221; d) X. Fang, K. McCallum, H. D. Pratt III, T. M. Anderson, K. Dennis, M. Luban, *Dalton Trans.* **2012**, *41*, 9867–9871.

[10] A. Giusti, G. Charron, S. Mazerat, J. D. Compain, P. Mialane, A. Dolbecq, E. Rivière, W. Wernsdorfer, R. N. Biboum, B. Keita, L. Nadjo, A. Filoramo, J. P. Bourgoin, T. Mallah, *Angew. Chem. Int. Ed.* **2009**, *48*, 4949–4952; *Angew. Chem.* **2009**, *121*, 5049–5052.

[11] a) S. T. Zheng, D. Q. Yuan, H. P. Jia, J. Zhang, G. Y. Yang, *Chem. Commun.* **2007**, 1858–1872; b) S. T. Zheng, D. Q. Yuan, J. Zhang, G. Y. Yang, *Inorg. Chem.* **2007**, *46*, 4569–4574; c) J. W. Zhao, J. Zhang, S. T. Zheng, G. Y. Yang, *Inorg. Chem.* **2007**, *46*, 10944–10946; d) J. W. Zhao, J. Zhang, S. T. Zheng, G. Y. Yang, *Chem. Commun.* **2008**, 570–572; e) S. T. Zheng, J. Zhang, G. Y. Yang, *Angew. Chem. Int. Ed.* **2008**, *47*, 3909–3913; *Angew. Chem.* **2008**, *120*, 3973–3977; f) J. W. Zhao, C. M. Wang, J. Zhang, S. T. Zheng, G. Y. Yang, *Chem. Eur. J.* **2008**, *14*, 9223–9239; g) S. T. Zheng, J. Zhang, J. M. Clemente-Juan, D. Q. Yuan, G. Y. Yang, *Angew. Chem. Int. Ed.* **2009**, *48*, 7176–7179; *Angew. Chem.* **2009**, *121*, 7312–7315; h) B. Li, J. W. Zhao, S. T. Zheng, G. Y. Yang, *Inorg. Chem.* **2009**, *48*, 8294–8303; i) S. T. Zheng, J. Zhang, X. X. Li, W. H. Fang, G. Y. Yang, *J. Am. Chem. Soc.* **2010**, *132*, 15102–15103; j) X. X. Li, S. T. Zheng, J. Zhang, W. H. Fang, G. Y. Yang, J. M. Clemente-Juan, *Chem. Eur. J.* **2011**, *17*, 13032–13043; k) L. Huang, J. Zhang, W. H. Fang, G. Y. Yang, *Chem. Commun.* **2012**, *48*, 9658–9660; l) L. Huang, S. S. Wang, J. W. Zhao, L. Cheng, G. Y. Yang, *J. Am. Chem. Soc.* **2014**, *136*, 7637–7642.

[12] a) P. J. Hagrman, D. Hagrman, J. Zubietua, *Angew. Chem. Int. Ed.* **1999**, *38*, 2638–2684; *Angew. Chem.* **1999**, *111*, 2798–2848; b) J. Gopalakrishnan, *Chem. Mater.* **1995**, *7*, 1265–1275; c) D. Hagrman, C. Sangregorio, C. J. O'Connor, J. Zubieta, *J. Chem. Soc. Dalton Trans.* **1998**, 3707–3710; d) H. Jin, Y. Qi, E. Wang, Y. Li, C. Qin, X. Wang, S. Chang, *Eur. J. Inorg. Chem.* **2006**, 4541–4545.

[13] G. Hervé, A. Tézé, *Inorg. Chem.* **1977**, *16*, 2115–2117.

[14] a) W. M. Wesley, W. G. H. Harry, *Reflectance Spectroscopy*, Wiley, New York, **1966**; b) J. I. Pankove, *Optical Processes in Semiconductors, Prentice-Hall*, New York, **1997**; c) Y. Xia, P. Wu, Y. Wei, Y. Wang, H. Guo, *Cryst. Growth Des.* **2006**, *6*, 253–257; d) L. Zhang, Y. Wei, C. Wang, H. Guo, P. Wang, *J. Solid State Chem.* **2004**, *177*, 3433–3438; e) Q. G. Zhai, X. Y. Wu, S. M. Chen, Z. G. Zhao, C. Z. Lu, *Inorg. Chem.* **2007**, *46*, 5046–5058.

[15] E. A. Axtell, Y. Park, K. Chondroudis, M. G. Kanatzidis, *J. Am. Chem. Soc.* **1998**, *120*, 124–136.

[16] G. C. Papavassiliou, *Prog. Solid State Chem.* **1997**, *25*, 125–270.

[17] I. D. Brown, D. Altermatt, *Acta Crystallogr. Sect. B* **1985**, *41*, 244–247.

[18] a) A. M. Ako, I. J. Hewitt, V. Mereacre, R. Clérac, W. Wernsdorfer, C. E. Anson, A. K. Powell, *Angew. Chem. Int. Ed.* **2006**, *45*, 4926–4929; *Angew. Chem.* **2006**, *118*, 5048–5051; b) R. T. W. Scott, S. Parsons, M. Murugesu, W. Wernsdorfer, G. Christou, E. K. Brechin, *Angew. Chem. Int. Ed.* **2005**, *44*, 6540–6543; *Angew. Chem.* **2005**, *117*, 6698–6701; c) R. Sessoli, H. L. Tsai, A. R. Schake, S. Wang, J. B. Vincent, K. Folting, D. Gatteschi, G. Christou, D. N. Hendrickson, *J. Am. Chem. Soc.* **1993**, *115*, 1804–1816.

[19] a) X. Y. Zhang, C. J. O'Connor, G. B. Jameson, M. T. Pope, *Inorg. Chem.* **1996**, *35*, 30–34; b) J. F. Liu, F. Ortega, M. T. Pope, *J. Chem. Soc. Dalton Trans.* **1992**, 1901–1906; c) X. Y. Zhang, C. J. O'Connor, G. B. Jameson, M. T. Pope, *Polyhedron* **1996**, *15*, 917–922; d) Z. M. Zhang, E. B. Wang, W. L. Chen, H. Q. Tan, *Aust. J. Chem.* **2007**, *60*, 284–290; e) S. G. Mitchell, P. I. Molina, S. Khanra, H. N. Miras, A. Prescimone, G. J. T. Cooper, R. S. Winter, E. K. Brechin, D. L. Long, R. J. Cogdell, L. Cronin, *Angew. Chem. Int. Ed.* **2011**, *50*, 9154–9157; *Angew. Chem.* **2011**, *123*, 9320–9323; f) P. Mialane, C. Duboc, J. Marrot, E. Rivière, A. Dolbecq, F. Secheresse, *Chem. Eur. J.* **2006**, *12*, 1950–1959; g) Q. Wu, Y. G. Li, Y. H. Wang, E. B. Wang, Z. M. Zhang, R. Clérac, *Inorg. Chem.* **2009**, *48*, 1606–1612; h) S. G. Mitchell, H. N. Miras, D. L. Long, L. Cronin, *Inorg. Chim. Acta* **2010**, *363*, 4240–4246; i) X. K. Fang, M. Luban, *Chem. Commun.* **2011**, *47*, 3066–3068; j) X. K. Fang, P. Kögerler, Y. Furukawa, M. Speldrich, M. Luban, *Angew. Chem. Int. Ed.* **2011**, *50*, 5212–5216; *Angew. Chem.* **2011**, *123*, 5318–5322.

[20] a) B. Moulton, M. J. Zaworotko, *Chem. Rev.* **2001**, *101*, 1629–1658; b) O. M. Yaghi, M. O'Keeffe, N. W. Ockwig, H. K. Chae, H. K. Chae, M. Eddaoudi, J. Kim, *Nature* **2003**, *423*, 705–714.

[21] a) E. Coronado, C. J. Gómez-García, *Chem. Rev.* **1998**, *98*, 273–296; b) N. Mizuno, M. Misono, *Chem. Rev.* **1998**, *98*, 199–218; c) P. Q. Zheng, Y. P. Ren, L. S. Long, R. B. Huang, L. S. Zheng, *Inorg. Chem.* **2005**, *44*, 1190–1192; d) J. W. Zhao, J. Cao, Y. Z. Li, J. Zhang, L. J. Chen, *Cryst. Growth Des.* **2014**, *14*, 6217–6229.

[22] D. Gatteschi, R. Sessoli, J. Villain, *Molecular Nanomagnets*, Oxford University Press, Oxford, **2006**.

[23] R. Sato, K. Suzuki, T. Minato, M. Shinoe, K. Yamaguchi, N. Mizuno, *Chem. Commun.* **2015**, *51*, 4081–4084.

[24] a) J. Krzystek, G.-J. Yeagle, J.-H. Park, R.-D. Britt, M.-W. Meisel, L.-C. Brunel, J. Telser, *Inorg. Chem.* **2003**, *42*, 4610–4618; b) J. Krzystek, A. Ozarowski, J. Telser, *Coord. Chem. Rev.* **2006**, *250*, 2308–2324.

[25] a) R. Ishikawa, R. Miyamoto, H. Nojiri, B. K. Breedlove, M. Yamashita, *Inorg. Chem.* **2013**, *52*, 8300–8302; b) A. Grigoropoulos, M. Pissas, P. Papatolis, V. Psycharis, P. Kyritsis, Y. Sanakis, *Inorg. Chem.* **2013**, *52*, 12869–12871; c) L. Chen, J. Wang, Y.-Z. Liu, Y. Song, X.-T. Chen, Y.-Q. Zhang, Z.-L. Xue, *Eur. J. Inorg. Chem.* **2015**, 271–278.

[26] A. P. Ginsberg, *Inorganic Synthesis Vol. 27*, Wiley, New York, **1990**, pp. 105–111.

[27] a) R. Acerete, J. Server-Carrió, *J. Am. Chem. Soc.* **1990**, *112*, 9386–9387; b) U. Kortz, M. G. Savelieff, B. S. Bassil, M. H. Dickman, *Angew. Chem. Int. Ed.* **2001**, *40*, 3384–3386; *Angew. Chem.* **2001**, *113*, 3488–3491; c) F. Robert, M. Leyrie, G. Hervfi, A. Tfizfi, Y. Jeannin, *Inorg. Chem.* **1980**, *19*, 1746–1752; d) M. Bösing, I. Loose, H. Pohlmann, B. Krebs, *Chem. Eur. J.* **1997**, *3*, 1232–1237.

Received: February 10, 2016

Published online on July 4, 2016